The Role of Forced Planetary Waves in the Annual Cycle of the Zonal Mean Circulation of the Middle Atmosphere[1]

J. R. HOLTON AND W. M. WEHRBEIN

Department of Atmospheric Sciences, University of Washington, Seattle 98195

(Manuscript received 20 February 1980, in final form 21 May 1980)

ABSTRACT

The annual cycle of the zonally averaged circulation in the middle atmosphere (16–96 km) is simulated using a severely truncated semi-spectral numerical model. The model includes only a single zonal harmonic wave component which interacts with the mean flow. The circulation is driven by diabatic heating and by a specified perturbation in the topography of the lower boundary, which is taken to be the 100 mb surface. Damping is included as Newtonian cooling and Rayleigh friction.

A comparison of the annual cycle simulated by this model with the results of an analogous two-dimensional model indicates that planetary waves have relatively little influence on the zonal mean temperature profiles and on the solstice mean zonal winds at high latitudes. The primary effects of the forced waves are in decelerating the mean winds in low latitudes in the winter hemisphere to produce a region of weak westerlies, and in generating "final warmings" at the spring equinoxes.

Computed mean zonal winds and wave amplitudes display significant hemispheric asymmetries. These differences are associated with the strong dependence of the eddy structure on the mean zonal wind profile.

The "residual" mean meridional circulation, computed by subtracting the portion of the Eulerian mean meridional flow which is exactly balanced by the eddy heat fluxes, is nearly identical at the solstices to the Eulerian mean circulation computed in the two-dimensional model. Except in low latitudes, the net mean flow forcing by the eddy fluxes is quite small at the solstices in agreement with the predictions of wave-mean flow non-acceleration theorems.

There are no major midwinter sudden warmings produced in the model. However, final warmings occur in the spring equinoctial seasons in both hemispheres. The rapid transient adjustments which occur during these final warmings make the equinoctial circulations in this model much different from the circulations computed for corresponding seasons in the two-dimensional model.

1. Introduction

Holton and Wehrbein (1980, hereafter referred to as HW) have recently used a two-dimensional primitive equation model to simulate the zonally symmetric circulation of the middle atmosphere (16–96 km). Their study demonstrated that the annual cycle in the observed zonal mean wind and temperature distributions in the upper stratosphere and mesosphere can, to a first approximation, be simulated using a zonally averaged model which does not include eddy heat and momentum fluxes due to forced planetary waves. HW found, however, that it is essential to include a parameterized mechanical damping of the mean flow near the mesopause in order to prevent the Coriolis torque associated with the diabatically driven mean meridional circulation from generating excessive mean zonal winds in the upper mesosphere.

The necessity for such a strong mechanical damping of the mean zonal wind in the mesosphere was first demonstrated by Leovy (1964). Leovy's model employed a linearized version of the zonally averaged quasi-geostrophic equations. He found that if a constant (height-independent) Rayleigh frictional damping was used in the zonal momentum equation, a rather short (~15 day) damping time was required in order to prevent the mean winds from becoming excessively strong in the mesosphere in both the winter and summer hemispheres. The results of HW and a similar study by Schoeberl and Strobel (1978) indicate, however, that strong damping is required only near the mesopause—not through the entire middle atmosphere. In fact, HW assumed a Rayleigh friction coefficient with a time constant $\gtrsim$ 80 days below 60 km, decreasing rapidly above that level to ~2 days at 80 km and above. HW postulated that the physical mechanism responsible for this strong damping is the turbulent breakdown of gravity waves near the mesopause. The wave drag generated by this breakdown should act

[1] Contribution No. 545, Department of Atmospheric Sciences, University of Washington.

0022-4928/80/091968-16$08.00

to relax the mean wind speed toward the phase speed of the waves. Thus, Rayleigh friction should mimic the tendency of topographically forced waves to relax the mean flow toward zero. Further indirect evidence of strong damping near the mesopause is provided by satellite observations which indicate that the mean amplitude of stationary planetary wavenumber 1 in the winter hemisphere decreases rapidly above ~60 km (Hirota and Barnett, 1977; Houghton, 1978).

The primary difference between the mean stratospheric circulation in the HW model and that produced by three-dimensional models is in the character of the mean meridional circulation. The HW model produces a solstice season mean meridional circulation in the stratosphere and mesosphere which is everywhere thermally direct. Mean rising motion over the summer pole and subsidence over the winter pole are coupled by a slow mean meridional drift from the summer hemisphere to the winter hemisphere. It is the adiabatic heating/cooling associated with this circulation which is responsible for the maintenance of a cold summer mesopause and a warm winter mesopause. However, observational studies (e.g., Mahlman, 1969) and three-dimensional models (e.g., Cunnold *et al.*, 1975) are not in accord with this simple one-cell solsticial mean meridional circulation pattern, at least in the stratosphere. In fact, the mean meridional circulation in the high-latitude stratosphere in winter is generally thermally *indirect*, with rising motion near the pole and compensating sinking in midlatitudes.

This thermally indirect mean meridional circulation is entirely due to the presence of large-amplitude vertically propagating planetary waves. The eddy momentum and heat fluxes associated with these planetary waves tend to destroy the thermal wind balance of the zonal mean flow (Holton, 1979, pp. 270–273), and drive a compensating mean meridional flow which continuously acts to maintain geostrophic balance. Therefore, the observed indirect mean meridional flow should be regarded as a *wave-driven* circulation. The compensation which exists between this wave-driven mean meridional flow and the eddy fluxes produced by the waves is expressed by the non-acceleration theorem[2] (Andrews and McIntyre, 1976; Boyd, 1976). In its Eulerian form this theorem states that, under suitable boundary conditions, nondissipative waves of steady amplitude will induce a mean meridional circulation which exactly cancels the eddy heat and momentum fluxes of the waves, so that the waves produce no net mean flow acceleration.

Although conditions in the stratosphere do not exactly satisfy the non-acceleration theorem, wave dissipation and wave transience are generally sufficiently small so that the eddy fluxes and the induced mean meridional circulation nearly cancel in the extratropical winter hemisphere, except during times of rapid changes in wave amplitude occurring at equinox or during sudden warming events. The HW model, which completely neglects eddy fluxes, is successful because the necessary conditions for the non-acceleration theorem are approximately met. Thus, the mean meridional circulation produced in the HW model should be regarded not as an approximation to the total Eulerian mean meridional circulation, but as representing the "residual" mean meridional flow which remains after the wave-driven flow is subtracted. During the solstice seasons when the temporal changes of the mean temperature are small this residual circulation is approximately just the *diabatic* circulation which balances the net radiative heating.

Despite the surprising success of the two-dimensional HW model, a number of important features of the observed general circulation of the middle atmosphere cannot be simulated without explicit inclusion of the forced stationary planetary wave disturbances which propagate vertically in the winter hemisphere. These features include the broad latitudinal extent of the equatorial semiannual oscillation, the strong asymmetry between vernal and autumnal equinox conditions, and the occurrence of mid-winter major and minor warmings.

In the present paper we report the results of a three-dimensional simulation which overcomes some of the deficiencies of the two-dimensional model. In order to isolate the role of forced stationary planetary waves, and to keep the model sufficiently simple to make annual cycle integrations feasible, we have chosen the minimum possible longitudinal resolution by including only a single zonal harmonic wave component (i.e., planetary wavenumber 1). As in HW the lower boundary is the 100 mb surface. The planetary wave disturbance is introduced by specifying a latitudinally dependent perturbation in the wavenumber 1 component of the topography of the lower boundary which is independent of time and symmetric about the equator. In reality, of course, there are seasonal variations in the strength of tropospheric planetary wave forcing, and differences between the hemispheres.

[2] Sometimes referred to as the "non-interaction" theorem. However, as Andrews and McIntyre (1978) have pointed out, there *is* an "interaction" between the waves and the mean flow in the sense that the waves drive a mean meridional circulation. However, this interaction does not drive a mean zonal wind acceleration. When the focus is on the potential temperature field the term "non-transport" theorem might be more suitable. However, for baroclinic motions in thermal wind balance the zonal mean potential temperature and wind fields are, of course, coupled through the thermal wind relation.

However, since one of our present objectives is to determine whether vacillations in the circulation can occur with constant forcing as the result of internal dynamical processes, we have chosen to specify a time-independent tropospheric forcing for the waves. However, it is important in simulating the annual cycle to include the variation of the zonal mean wind at the 100 mb level. Thus, as in HW, we have here set the zonal mean 100 mb heights to vary as observed by fitting the first two harmonics of the annual cycle to the climatological data (see HW for details). The present experiment, therefore, is designed to examine the annual cycle of the large-scale circulation in the middle atmosphere in the presence of constant tropospheric planetary wave forcing.

2. The dynamical model

The model is based on the primitive equations in log-pressure coordinates (Holton, 1975). To avoid simulating the tropospheric circulation the lower boundary is set at the 100 mb level and the effects of tropospheric forcing are included in the lower boundary condition as outlined in the previous section. The upper boundary is placed at 96 km and the latitudinal extent is global.

The basic equations in this system are given in Holton (1975) and Holton and Wehrbein (1979).[3] In order to develop the semi-spectral model the basic equations are expanded in zonal harmonic series by letting

$$f(\lambda,y,z,t) = e^{z/2H}\sum_{n=-\infty}^{n=+\infty} F_n(y,z,t)e^{in\lambda}, \qquad (1)$$

where λ is longitude, $f(\lambda,y,z,t)$ stands for any field variable, and F_n is the Fourier transform of f. All dependent variables are expanded in Fourier series as in (1) and the series are then truncated to retain only the zonal mean ($n = 0$) and a single planetary wave component ($n = s$) to obtain the set of prognostic equations.

a. Zonal mean equations

If we designate the $n = 0$ variables by overbars, the zonal mean equations can be written

$$\frac{\partial\bar{U}}{\partial t} - f\bar{V} = -e^{z/2H}\left[\frac{1}{\cos^2\theta}\frac{\partial}{\partial y}(\bar{U}\bar{V}\cos^2\theta) + \frac{\partial}{\partial z}(\bar{U}\bar{W})\right] - \kappa_R\bar{U} + F_M + D_1(\bar{U}), \qquad (2)$$

$$\frac{\partial\bar{V}}{\partial t} + f\bar{U} = -\frac{\partial\bar{\Psi}}{\partial y} - e^{z/2H}\bar{U}^2a^{-1}\tan\theta + D_2(\bar{V}) - \kappa_R\bar{V}, \qquad (3)$$

$$\frac{1}{\cos\theta}\frac{\partial}{\partial y}(\bar{V}\cos\theta) + \left(\frac{\partial}{\partial z} - \frac{1}{2H}\right)\bar{W} = 0, \qquad (4)$$

$$\frac{\partial}{\partial t}\left(\frac{\partial\bar{\Psi}}{\partial z} + \frac{\bar{\Psi}}{2H}\right) + N^2\bar{W} = F_T - e^{z/2H}\left\{\frac{1}{\cos\theta}\frac{\partial}{\partial y}\left[\bar{V}\cos\theta\left(\frac{\partial}{\partial z} + \frac{1}{2H}\right)\bar{\Psi}\right] + \frac{\partial}{\partial z}\left[\bar{W}\left(\frac{\partial}{\partial z} + \frac{1}{2H}\right)\bar{\Psi}\right]\right\} + D_2\left(\frac{\partial\bar{\Psi}}{\partial z} + \frac{\bar{\Psi}}{2H}\right) + \bar{Q}. \qquad (5)$$

Here κ_R is the Rayleigh friction coefficient, $D_1(\ )$ and $D_2(\ )$ are defined in Section 2d, F_M and F_T denote the eddy momentum and eddy heat flux convergences, respectively, $\bar{Q}$ denotes the diabatic heating, $\bar{\Psi}$ is the zonal mean geopotential, and all other symbols have their conventional meanings. Upper case symbols are used for the velocity components to clearly indicate that (2)–(5) involve the Fourier transformed variables which are weighted by the square root of the basic-state density $e^{-z/2H}$. We have neglected the advection by the mean meridional flow and the eddy flux terms in (3) because the mean zonal wind is nearly in gradient wind balance.

With the aid of (4) we can define a mean meridional streamfunction $\bar{X}$ by letting

$$\bar{W}\cos\theta = \partial\bar{X}/\partial y,$$

$$\bar{V}\cos\theta = -\left(\frac{\partial}{\partial z} - \frac{1}{2H}\right)\bar{X}. \qquad (6)$$

The $\bar{X}$ field is useful in specifying boundary conditions and in solving the zonal mean component equations.

The eddy flux convergence terms in (2) and (5) may be written as

$$F_M \equiv -e^{z/2H}\left\{\frac{1}{\cos^2\theta}\frac{\partial}{\partial y}[(U_SV_S^* + U_S^*V_S)\cos^2\theta] + \frac{\partial}{\partial z}(U_SW_S^* + U_S^*W_S)\right\}, \qquad (7)$$

$$F_T \equiv -e^{z/2H}\left\{\frac{1}{\cos\theta}\frac{\partial}{\partial y}\left[\cos\theta\left[V_S\left(\frac{\partial}{\partial z} + \frac{1}{2H}\right)\Psi_S^* + V_S^*\left(\frac{\partial}{\partial z} + \frac{1}{2H}\right)\Psi_S\right]\right] + \frac{\partial}{\partial z}\left[W_S^*\left(\frac{\partial}{\partial z} + \frac{1}{2H}\right)\Psi_S + W_S\left(\frac{\partial}{\partial z} + \frac{1}{2H}\right)\Psi_S^*\right]\right\}, \qquad (8)$$

[3] Holton, J. R., and W. M. Wehrbein, 1979: A semi-spectral numerical model for the large scale stratospheric circulation. Rep. No. 1, Middle Atmosphere Project, Dept. of Atmospheric Sciences, University of Washington.

where the S subscripts denote the Fourier transformed wave fields and the asterisks denote complex conjugates.

b. Eddy equations

The Fourier coefficients in the eddy flux terms (7) and (8) are determined from the eddy equations

$$\frac{\partial U_S}{\partial t} - fV_S = \frac{-iS\Psi_S}{a\cos\theta} - e^{z/2H}\left[\frac{iSU_S\bar{U}}{a\cos\theta} + \frac{V_S}{\cos\theta}\frac{\partial}{\partial y}(\bar{U}\cos\theta) + W_S\left(\frac{\partial}{\partial z} + \frac{1}{2H}\right)\bar{U}\right] - \kappa_R U_S + D_2(U_S), \quad (9)$$

$$\frac{\partial V_S}{\partial t} + fU_S = -\frac{\partial \Psi_S}{\partial y} - e^{z/2H}\left(\frac{2\bar{U}U_S\tan\theta}{a} + \frac{iSV_S\bar{U}}{a\cos\theta}\right) - \kappa_R V_S + D_2(V_S), \quad (10)$$

$$\frac{\partial}{\partial t}\left[\left(\frac{\partial}{\partial z} + \frac{1}{2H}\right)\Psi_S\right] + N^2W_S = Q_S - e^{z/2H}\left\{\left[\frac{iS\bar{U}}{a\cos\theta}\left(\frac{\partial}{\partial z} + \frac{1}{2H}\right)\right]\Psi_S + W_S\left(\frac{\partial}{\partial z} + \frac{1}{2H}\right)^2\bar{\Psi} + V_S\frac{\partial}{\partial y}\left(\frac{\partial}{\partial z} + \frac{1}{2H}\right)\bar{\Psi}\right\} + D_2\left[\left(\frac{\partial}{\partial z} + \frac{1}{2H}\right)\Psi_S\right], \quad (11)$$

$$\frac{iSU_S}{a\cos\theta} + \frac{1}{\cos\theta}\frac{\partial}{\partial y}(\cos\theta V_S) + \left(\frac{\partial}{\partial z} - \frac{1}{2H}\right)W_S = 0. \quad (12)$$

Here all terms involving advection by the mean meridional circulation $(\bar{V},\bar{W})$ have been neglected.

c. Boundary conditions

For the zonal mean the boundary conditions at the poles are

$$\bar{X} = \bar{U} = \bar{V} = \partial\bar{\Psi}/\partial y = 0, \quad \theta = \pm\pi/2. \quad (13)$$

For the eddy equations similar conditions apply except that the case $S = 1$ must be treated separately because U_S and V_S do not vanish at the poles for wavenumber one. Thus the appropriate conditions at $\theta = \pm\pi/2$ are

$$\left.\begin{aligned} &\Psi_S = 0, && \text{all } S\\ &U_S = V_S = 0, && S > 1\\ &\partial U_S/\partial y = \partial V_S/\partial y = 0, && S = 1 \end{aligned}\right\}. \quad (14)$$

At the lower boundary the zonal mean flow is assumed to be in gradient wind balance so that

$$\left.\begin{aligned} &\bar{U} = \bar{U}_B(y,t)\\ &\bar{V} = 0\\ &-\frac{\partial\bar{\Psi}}{\partial y} = f\bar{U}_B + \bar{U}_B{}^2\frac{\tan\theta}{a}e^{z/2H} \end{aligned}\right\}, \quad (15)$$

where $\bar{U}_B(y,t)$ is specified from observations.

At the upper boundary ($z = z_T$) we assume that the vertical shears of the mean zonal wind, the mean meridional wind and the mean geopotential vanish. Thus,

$$\frac{\partial}{\partial z}(\bar{U}e^{z/2H}) = \left(\frac{\partial}{\partial z} + \frac{1}{2H}\right)\bar{U} = 0, \quad (16a)$$

$$\left(\frac{\partial}{\partial z} + \frac{1}{2H}\right)\bar{V} = 0, \quad (16b)$$

$$\left(\frac{\partial}{\partial z} + \frac{1}{2H}\right)\bar{\Psi} = 0. \quad (16c)$$

Condition (16c) implies that the zonal mean temperature *must* equal the basic state temperature $T_0(z)$ at $z = z_T$.

In addition to conditions (15) and (16) boundary conditions are required for the vertical momentum and heat fluxes associated with the mean meridional circulation. We wish to avoid specifying $\bar{W}$ or the fluxes themselves at $z = 0$. Instead, we assume that the flux divergences vanish at the lower boundary, i.e.,

$$\frac{\partial}{\partial z}(\bar{U}\bar{W}) = \frac{\partial}{\partial z}\left[\bar{W}\left(\frac{\partial}{\partial z} + \frac{1}{2H}\right)\bar{\Psi}\right] = 0. \quad (17)$$

However, for simplicity we assume that the fluxes themselves vanish at the upper boundary. If, in addition, we let $\bar{Q} = F_T = 0$ at $z = z_T$, then from (5) we have $\bar{W} = 0$ at $z = z_T$.

For the eddy equations boundary conditions at $z = 0$, z_T are required only for the geopotential perturbation. At the lower boundary we specify a stationary geopotential height perturbation, which is symmetric about the equator,

$$\Psi_S(y) = \begin{cases} gh_B\sin^2(3\theta - \pi/2) \\ \quad\times\exp(-i|\theta|), & |\theta| > \pi/6 \\ 0, & |\theta| \leq /6 \end{cases} \quad (18)$$

where $h_B = 150$ m. The phase tilt in latitude is included to simulate the observed mean poleward eddy momentum flux at the 100 mb level.

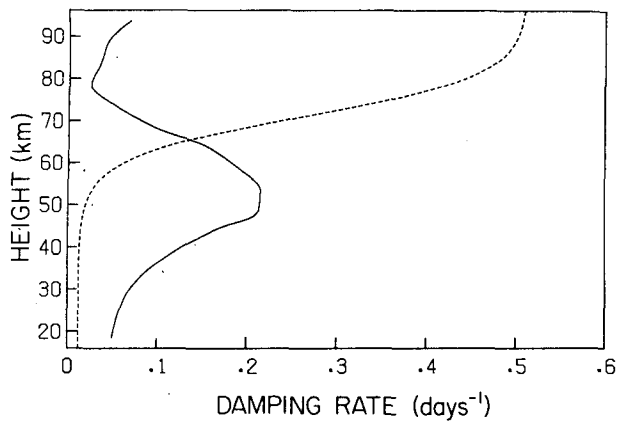

FIG. 1. Vertical profiles of Newtonian cooling coefficient (solid line) and Rayleigh friction coefficient (dashed line), both in units of day^{-1}.

This forcing, which is similar to the distribution used by Matsuno (1971) in his stratospheric warming simulations, is somewhat larger than the climatological mean value for Northern Hemisphere winter. We have deliberately chosen to impose a strong wave forcing in order to emphasize possible wave-mean flow interaction effects on the zonal mean flow.

At the upper boundary the wave perturbations are assumed to vanish,

$$\Psi_S = 0 \quad \text{at} \quad z = z_T. \tag{19}$$

This condition requires that we impose strong damping in the layer near z_T to prevent spurious reflection of wave energy from the upper boundary. Finally, in order to compute F_M and F_T at the upper and lower boundaries we assume that the vertical momentum and heat flux divergences vanish at the boundaries.

d. Subgrid-scale diffusion

In order to suppress nonlinear instability in the course of the numerical calculations it proved necessary to apply a weak meridional smoothing to the $\bar{U}$, $\bar{V}$ and $\bar{\Psi}$ fields. To prevent this smoothing from damping the large-scale motions we have chosen a highly scale-dependent biharmonic diffusion. Thus the operator $D_2(\ )$ in Eqs. (3), (5), (9), (10) and (11) is defined as

$$D_2(\ ) \equiv -\frac{K}{\cos\theta}\frac{\partial^4(\ )}{\partial y^4},$$

where K is a constant with units of m^4 s^{-1}. The diffusion operator $D_1(\ )$ in (2) must be defined in a special way so that the subgrid-scale horizontal diffusion conserves relative angular momentum on an isobaric surface, and also acts as a net energy sink. The required form of diffusion is

$$D_1(\bar{U}) = -\frac{K}{\cos^2\theta}\frac{\partial^4}{\partial y^4}\left(\frac{\bar{U}}{\cos\theta}\right)$$

so that relative angular velocity is diffused. In the present model we have set $K/\Delta y^4 = 10^{-7}$ s^{-1} which implies a decay time of about 4 days for two grid-length waves and 64 days for four grid-length waves.

e. Rayleigh friction parameterization

Mechanical damping is introduced in the simplest possible manner as a height-dependent Rayleigh friction with rate coefficient given by

$$\kappa_R = \kappa_0 + \kappa_1\left[1 + \tanh\left(\frac{z - 71.}{10.}\right)\right],$$

where $\kappa_0 = 1/(80$ days), $\kappa_1 = 1/(4$ days) and z is in kilometers. The profile of κ_R is shown in Fig. 1.

f. Solar heating

Ozone is the only important absorber of solar radiation in the middle atmosphere. The diurnally averaged solar heating due to absorption by ozone is computed in the model by fixing the sun angle at its average value between sunrise and sunset [approximation 1 of Cogley and Borucki (1976)] for the daylight fractional part of a day. Both sun angle and daylight fraction are known functions of latitude and time of year. The parameterization of Lacis and Hansen (1974) is used to compute the solar heating. We have assumed that the ozone profile is a specified function of height alone in this calculation. Thus, the solar heating in the Northern Hemisphere differs from that in the Southern Hemisphere one-half year earlier (or later) only by the small factor due to the ellipticity of the earth's orbit.

g. Infrared cooling

We have employed Dickinson's (1973) parameterization of infrared cooling which consists of the sum of the cooling for a reference atmosphere of temperature $T_0(z)$ and a Newtonian cooling approximation for temperature departures from the reference profile. Determination of the cooling for the reference state is discussed in HW. The Newtonian cooling profile for the temperature departure field which we have used is shown in Fig. 1. The values in the 30–80 km range are those given by Dickinson (1973). Below 30 km Trenberth's (1973) values are used. Following Schoeberl and Strobel (1978) the value of the Newtonian cooling coefficient between 80 and 96 km was estimated as the CO_2 cooling rate in the fundamental band at 15 μm.

3. The numerical model

The finite-difference analogue to the dynamical system described in the previous section has been described in detail by Holton and Wehrbein (1979).[3] Briefly, the model employs a staggered grid in the meridional plane with a grid spacing of 10° in latitude and 5 km in height. The time-differencing scheme is based on a modification of the semi-implicit time differencing used in HW. In the semi-implicit scheme the linear terms in dynamical equations are represented by time-averaged values defined by the relationship

$$\hat{F} = \tfrac{1}{2}\gamma(F^{n+1} + F^{n-1}) + (1 - \gamma)F^n, \qquad (20)$$

where n designates the nth time step and γ is a weighting factor. HW set $\gamma = \frac{1}{2}$, but in the present model that choice led to computational instability. Simmons *et al.* (1978) showed that this type of instability often appears in the semi-implicit scheme when the actual temperature profile deviates by a large amount from the reference profile (in our case the U.S. Standard Atmosphere), but could be eliminated by using a larger value for γ. In the present study we have set $\gamma = 3$ and used a time step of 1 h except during periods of enhanced wave activity when a time step of 30 min was required.

4. The simulated annual cycle

The model was initialized for solar conditions corresponding to the Northern Hemisphere vernal equinox. The initial temperature field was set equal to the reference temperature $T_0(z)$. In order to satisfy the thermal wind equation, the initial mean zonal flow was then specified to be a barotropic flow equal at all heights to the mean wind specified at the lower boundary, $U_B(y)$. The planetary wavenumber 1 disturbance was initially set to zero and allowed to exponentially approach its steady-state value with e-folding time of 4 days.

For convenience the annual period was assumed to be 360 days. The simulation was carried forward for a total of 590 days in order to detect any significant interannual variation. After a transient adjustment period of ~60 days the zonal mean and eddy circulations both settled into an annual cycle in which even short period variations repeated every 360 days as shown, for example, by Fig. 2.

a. Zonal mean temperature

The variation of the polar stratopause (48.5 km level) temperatures as a function of time for the entire duration of the model run is shown in Fig. 2. The overall annual temperature variation in this simulation is remarkably similar to that of the two-dimensional HW model except during the spring

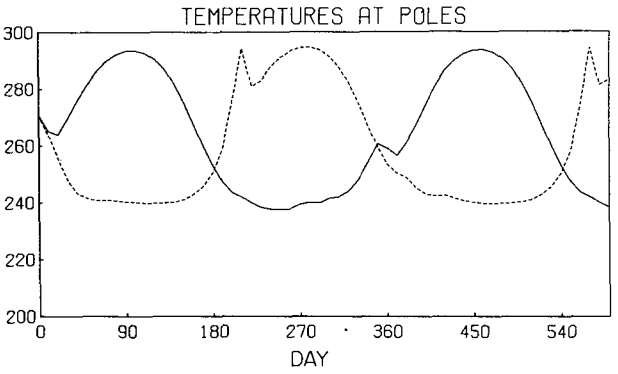

FIG. 2. Time evolution of the temperatures (K) at the polar stratopause (48.5 km) for the Northern Hemisphere (solid line) and Southern Hemisphere (dashed line).

equinoctial periods. In the HW model the temperature at the pole increased monotonically in the period from the spring equinox to the summer solstice, with no significant differences between the two hemispheres. However, in the present model "spikes" in the temperature field occur during the spring equinoctial season in both hemispheres. However, there are important differences in the timing and amplitude of the spikes. In the Northern Hemisphere a brief temperature maximum, corresponding to a weak late winter sudden warming, occurs about 10 days prior to the equinox. In the Southern Hemisphere, a much stronger temperature maximum occurs ~30 days following the equinox. As we shall see this latter temperature event is due to wave-mean flow interaction associated with wave transience (Andrews and McIntyre, 1976).

The annual cycle of the zonal mean temperature field above 10 mb is as yet not well documented. Barnett (1974) has analyzed the equivalent radiance temperatures for four channels of the Selective Chopper Radiometer on Nimbus 4 for the period 15 November 1970 to 15 November 1971. The results for channel A, which has a weighting function with a peak at about 43 km and a half-width of ~20 km, are shown in terms of equivalent blackbody temperatures in Fig. 3a, while the analogous field for the model simulation is shown in Fig. 3b. In preparing Fig. 3b we have computed weights for each model level between 23.5 and 68.5 km from Barnett's channel A weighting function and computed the appropriate weighted-average model temperatures.

Temperatures in the model tend to be lower than the observed by ~5–10 K in the equatorial region throughout the year, and by ~5 K at the southern summer solstice pole and ~10 K at the northern summer solstice pole. The model does not exhibit the short time scale transient features shown by the data—particularly the midwinter sudden

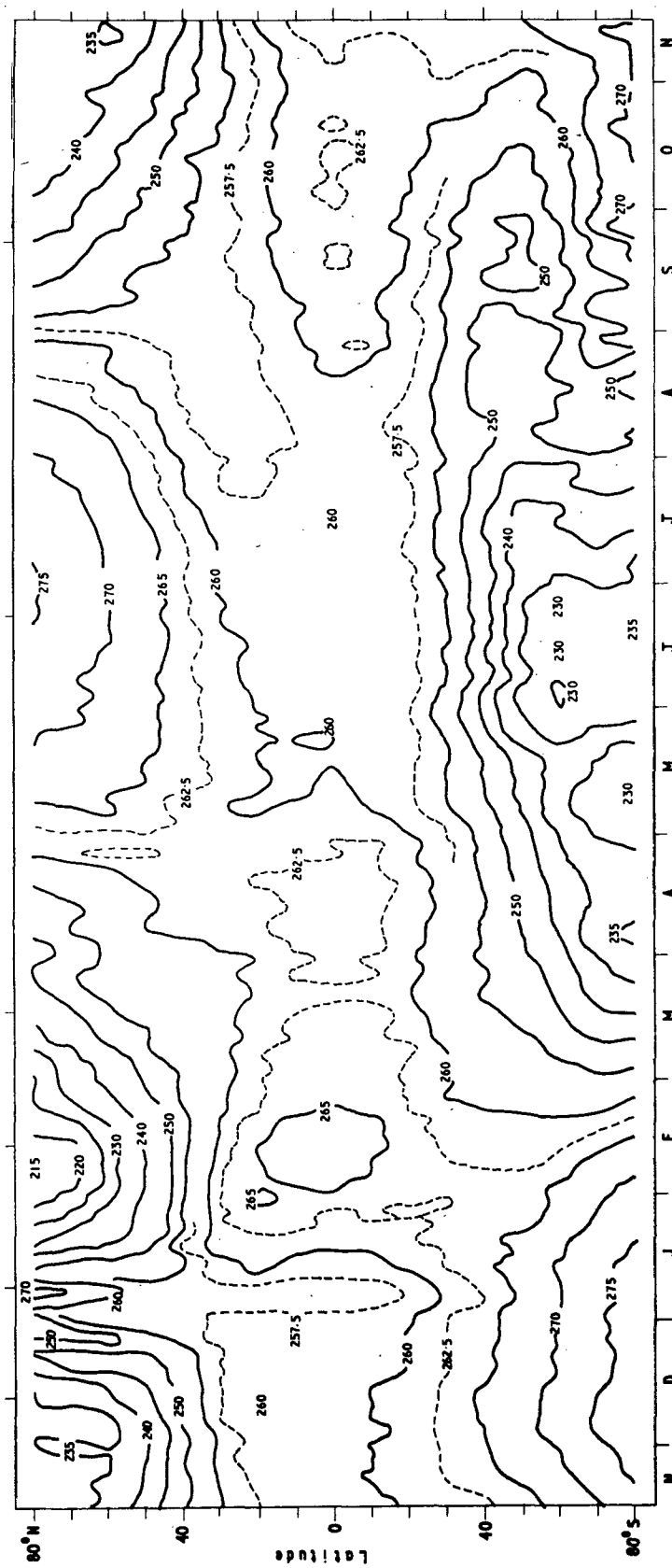

FIG. 3a. Latitude-time sections of temperature (K) equivalent to zonal mean of radiance for Channel A of the Nimbus 4 SCR. Averaging was performed over 10° wide latitude bands (Barnett, 1974).

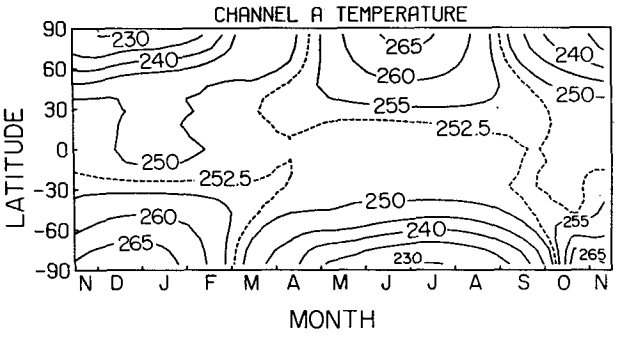

FIG. 3b. Model derived zonal mean Channel A temperature (K).

warming in the Northern Hemisphere which peaks about 8 January 1971. However, the overall correspondence between model and observation is quite striking. In both cases cold temperatures spread equatorward slowly from the southern pole in autumn and retreat rapidly in spring, while in the Northern Hemisphere cold temperatures advance rapidly from the autumn pole, but retreat slowly in the spring. These differences are explained by the different behavior of the planetary waves in the Northern and Southern Hemispheres as will be described in Section 4c.

Fig. 4 shows the zonal mean temperature distribution for the Northern Hemisphere summer solstice. The profile for the Northern Hemisphere winter solstice is nearly a mirror image of Fig. 4 so it will not be shown. The solstice season temperature profile is also in very close agreement with the profile produced by the HW two-dimensional model (cf. HW Fig. 8) except in the lower stratosphere where the present model succeeds in simulating the midlatitude temperature maximum in the winter hemisphere. The strong similarity between the solstice temperature profile of Fig. 4 and that produced by the HW model supports the assertion of HW that the approximate validity of the Andrews-McIntyre (1976) non-acceleration theorem makes it possible to model the zonal mean circulation of the middle atmosphere to a first approximation without explicitly including eddy heat fluxes. In the absence of transient wave activity, the eddy heat fluxes are nearly cancelled by their induced mean meridional circulation so that the diabatic circulation primarily determines the temperature profile. Although both thermal and mechanical wave damping are present the vertical scale of the damping (and hence the mean flow deceleration) is sufficiently large so that changes in the vertical shear of the mean wind are small at middle and high latitudes. Thus, from thermal wind considerations, changes in the meridional temperature gradient must be small and the wave damping has little influence on the temperature profile.

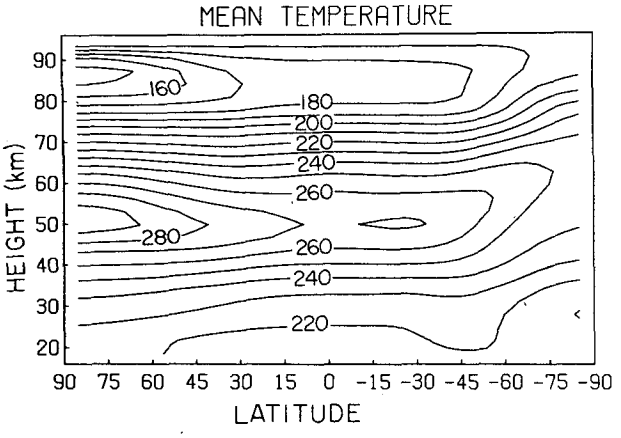

FIG. 4. Latitude-height section of mean temperature at Northern Hemisphere summer solstice.

The situation for the equinoxes is not quite so simple. The temperature profile for the Northern Hemisphere autumnal equinox (Fig. 5) is nearly identical to the corresponding season in the HW model, except for the midlatitude temperature maximum in the lower stratosphere. At the Northern Hemisphere spring equinox, however, the temperature profile (Fig. 6) deviates substantially from that of the HW model in the high latitudes of the Northern Hemisphere. This difference may be attributed to the weak sudden stratospheric warming which occurs just prior to the spring equinox and causes a temperature reversal poleward of 60°N. Thus at this particular time the dynamical influence of the forced wave disturbance contributes significantly to the mean temperature distribution.

In summary, the overall annual zonal mean temperature cycle is not very strongly influenced by the presence of forced planetary waves, although in high latitudes the waves can produce substantial short-term local deviations from the results of the two-dimensional model.

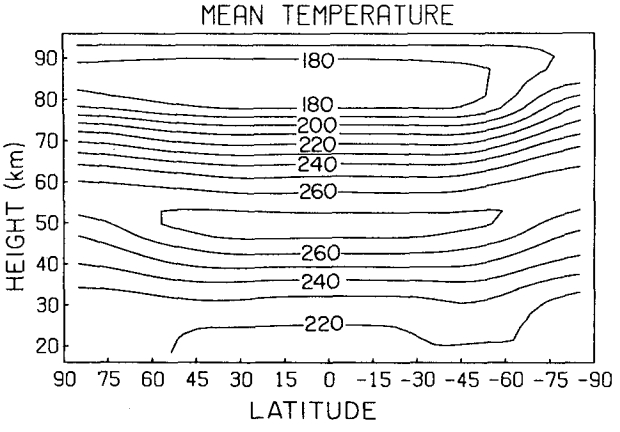

FIG. 5. Latitude-height section of mean temperature at Northern Hemisphere autumnal equinox.

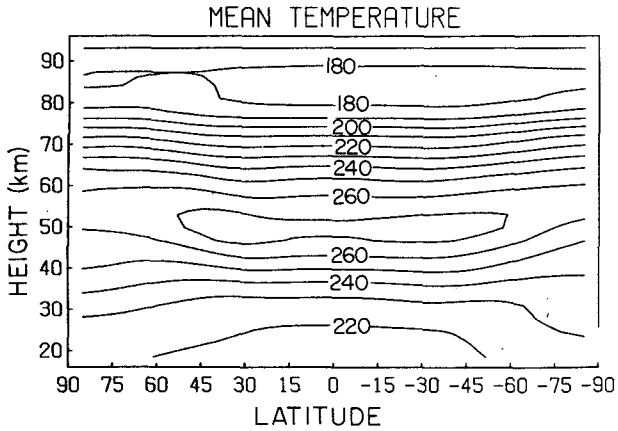

FIG. 6. Latitude-height section of mean temperature at Northern Hemisphere vernal equinox.

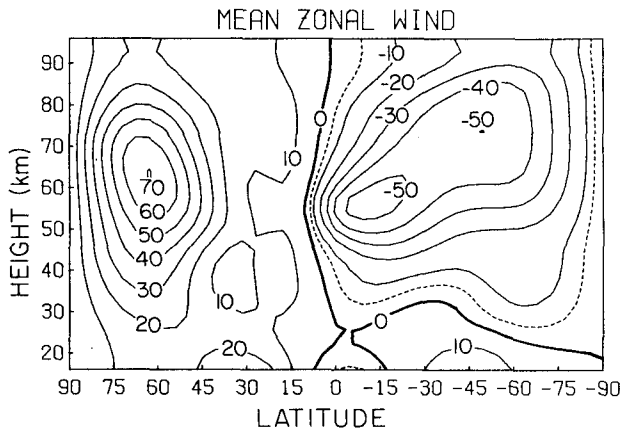

FIG. 8. Mean zonal wind at Northern Hemisphere winter solstice.

b. *Mean zonal wind*

Mean zonal wind profiles for all four seasons are shown in Figs. 7–10. These wind profiles are substantially different from the corresponding profiles in HW. However, since in all seasons except the Northern Hemisphere spring equinox the differences are primarily limited to low latitudes, and have large vertical scales, only small temperature differences are needed to preserve thermal wind balance. Thus, the temperature profiles in the present model show much greater similarity to the HW results than do the wind profiles.

An examination of the balance of terms in the zonal mean momentum equation reveals that it is the horizontal momentum fluxes due to the winter hemisphere planetary waves which account for the differences between the low-latitude solstice wind profiles of HW and those of the present model. Although the momentum flux divergence is nearly cancelled by the Coriolis torque of the mean meridional flow, the presence of damping and wave transience causes a net easterly acceleration in low latitudes and westerly acceleration in high latitudes. As a result the summer hemisphere easterlies are slightly stronger than in HW while the westerly jets have moved about 15° poleward from their positions in the HW model.

Although the mean zonal winds in the two solstice seasons have an approximate mirror symmetry about the equator, comparison of Fig. 8 with Fig. 10 indicates that the Northern winter westerly jet is ~ 10 m s^{-1} weaker than the jet in the southern winter. This weaker jet must be caused by the planetary wave disturbance, but must itself also *influence* the amplitude and phase of the stationary wave since planetary wave propagation is strongly influenced by mean zonal wind profile.

Due to the sudden stratospheric warming at the time of the Northern Hemisphere spring equinox, the mean zonal winds in spring are much different in the Northern and Southern Hemispheres (Figs. 7 and 9). During the Southern Hemisphere spring

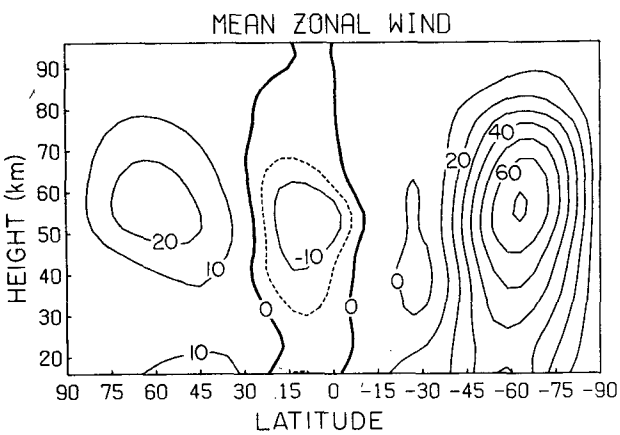

FIG. 7. Mean zonal wind at Northern Hemisphere autumnal equinox.

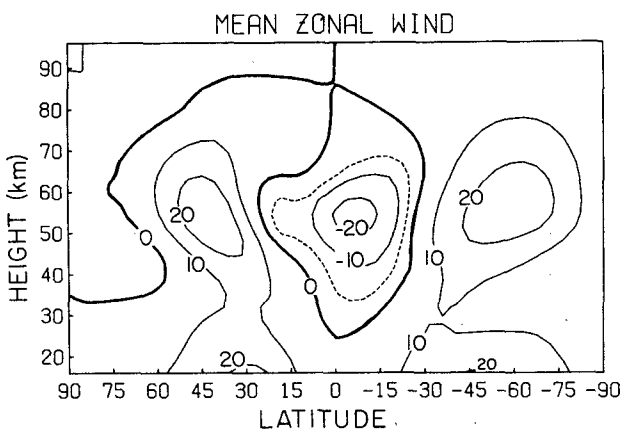

FIG. 9. Mean zonal wind at Northern Hemisphere vernal equinox.

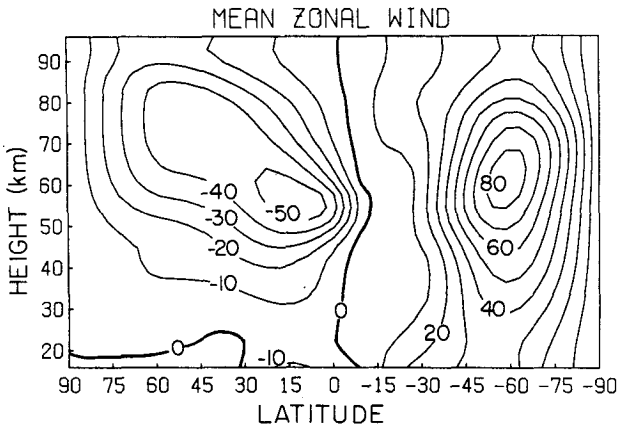

FIG. 10. Mean zonal wind at Northern Hemisphere summer solstice.

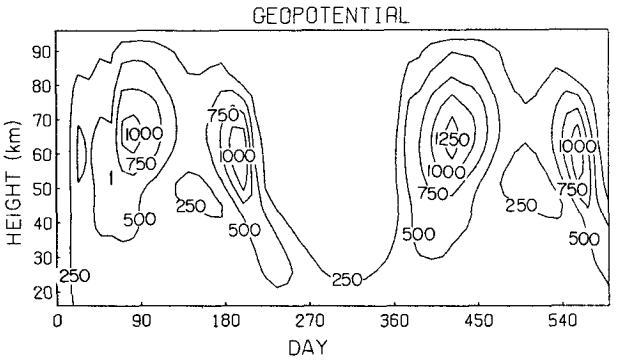

FIG. 12. Amplitude (m) of geopotential perturbation for wavenumber 1 at 60°S vs model day.

the results of the present model are similar to those of HW, although the westerly jet in the Southern Hemisphere is stronger and nearer the pole than that in HW. However, in the northern spring the mean zonal wind is actually easterly in the high-latitude stratosphere and only very weak westerlies remain at middle latitudes.

c. *Eddy geopotential disturbance*

Figs. 11 and 12 show time-height sections of the amplitude of the planetary wavenumber 1 disturbance at 60°N and 60°S, respectively. In both hemispheres the wave propagation is suppressed during the summer easterlies in agreement with the Charney-Drazin (1961) criterion. Strong wave activity occurs in both winter hemispheres. However, in the northern winter the waves have only small amplitude variations until the time of the late winter final warming when there is a rapid collapse of the waves as the mean wind switches to easterly. In the Southern Hemisphere, on the other hand, the wave amplitude is strongest in late spring and early autumn, and has a relative minimum during the winter when the mean zonal winds are strongest. Since the amplitude of the forced wave disturbance at the lower boundary is the same in both hemispheres, the differences in wave propagation must be due to the differences in the mean zonal flow. Holton and Dunkerton (1978) found that in a β-plane channel model planetary wave propagation was very sensitive to the mean wind profile. Since the vertical shear of the mean wind is similar in the two hemispheres it is evident that the dramatic difference in wave propagation is due to the stronger imposed mean zonal wind at the 100 mb level in the southern winter (cf. Figs. 8 and 10).

Profiles of the amplitude and phase of the geopotential perturbation at the equinoxes and solstices are shown in Figs. 13–16. During the equinoxes and winter solstices when the mean zonal winds are westerly, strong wave disturbances are present. The waves tilt westward with height as required for poleward heat fluxes, and westward toward the equator as required for poleward momentum fluxes.

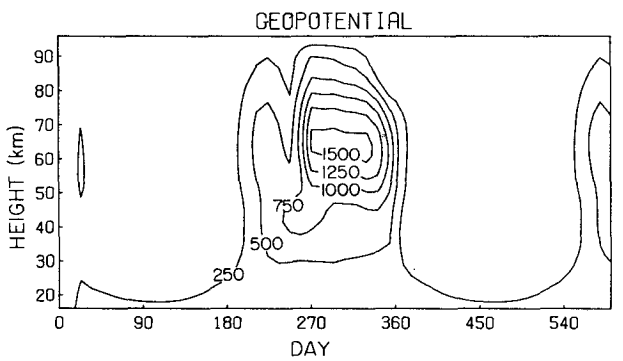

FIG. 11. Amplitude (m) of geopotential perturbation for wavenumber 1 at 60°N vs model day.

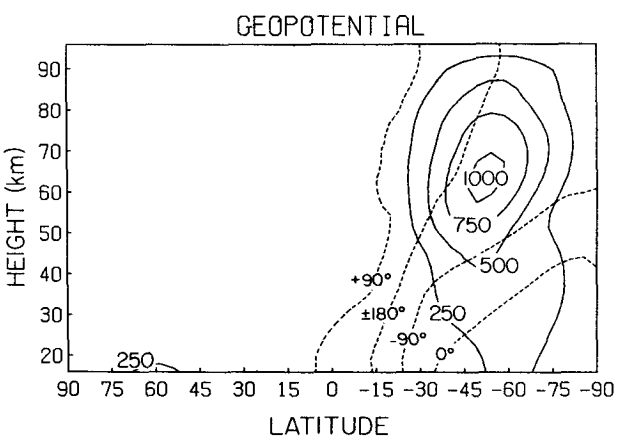

FIG. 13. Amplitude in meters (solid line) and longitude of ridge line (dashed line) of wave geopotential perturbation at Northern Hemisphere summer solstice.

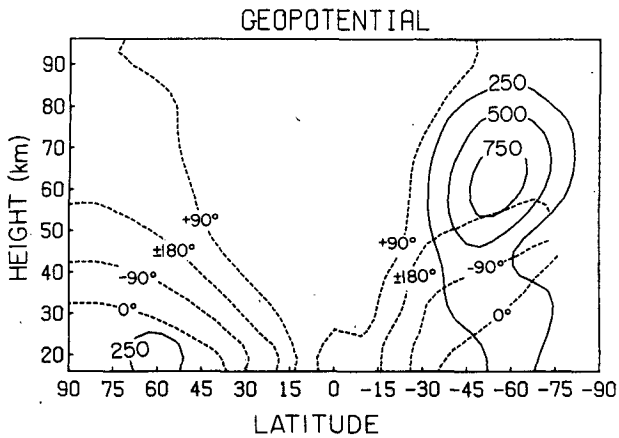

FIG. 14. As in Fig. 12, except at Northern Hemisphere autumnal equinox.

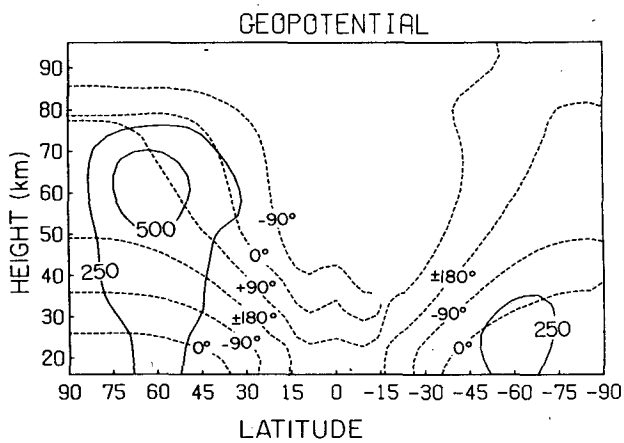

FIG. 16. As in Fig. 12, except at Northern Hemisphere vernal equinox.

The maximum amplitude occurs near the 60 km level and the waves decay rapidly above that level in agreement with observations (Hirota and Barnett, 1977; Houghton, 1978). In an earlier version of this model in which the mechanical dissipation was independent of height, the wave amplitude was a maximum at the highest level of the model. The more realistic amplitude distribution in the present model may be regarded as further evidence for the existence of strong mechanical dissipation near the mesopause.

d. Mean meridional circulation

As noted above, the planetary wave disturbance induces a mean meridional circulation which tends to cancel the eddy heat and momentum flux divergences due to the waves. Hence, the Eulerian mean meridional circulation in the present model must be much different from that in the HW two-dimensional model. This is illustrated by Figs. 17 and 18 which show the mean meridional wind and the mean vertical velocity for the Northern Hemisphere summer solstice. The single-cell direct thermal circulation of the HW model is here replaced by a two-cell circulation below ~60 km in which a second thermally indirect cell has been added in the high latitudes of the winter hemisphere. However, as we shall show in the next section the adiabatic cooling due to this Eulerian mean motion near the winter pole is completely cancelled by an eddy heat flux convergence. The actual Lagrangian motion of individual fluid parcels must be downward in this region of strong diabatic cooling (Dunkerton, 1978; Wallace, 1978), despite the upward directed Eulerian mean motion.

The situation at the equinoxes is similar although the actual mean meridional motion pattern is more complex due to the presence of wave activity in both hemispheres. There are thermally indirect cells in the high latitudes of both hemispheres (stronger in the spring hemisphere) which are super-

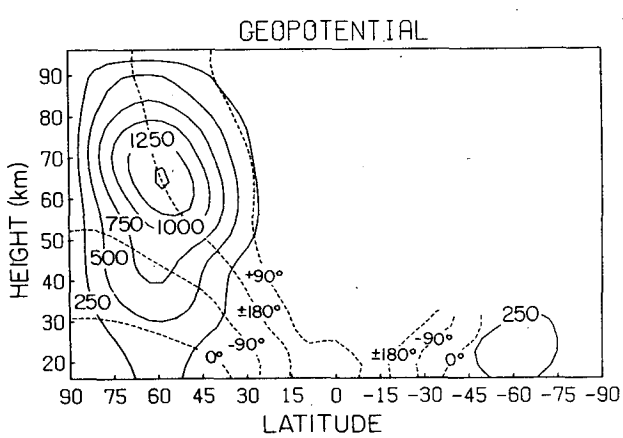

FIG. 15. As in Fig. 12, except at Northern Hemisphere winter solstice.

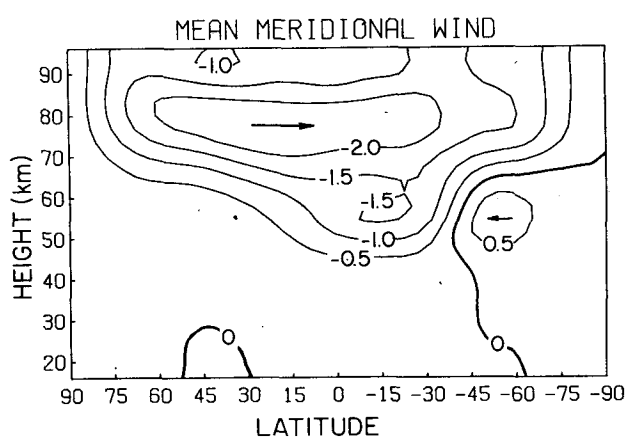

FIG. 17. Mean meridional wind (m s^{-1}) at Northern Hemisphere summer solstice.

posed on the diabatic circulation of HW which has rising in the equatorial region and sinking at high latitudes.

In summary, the mean meridional circulation is greatly changed by the presence of the eddies. However, meaningful statements about the roles of the mean meridional circulation in the heat and momentum budgets can only be made when the wave-driven part of the mean meridional circulation is separated out.

5. A diagnosis of the mean flow forcing by planetary wave disturbances

As we have already seen, the role of the planetary wave momentum and heat fluxes in the annual cycle of the zonal mean circulation cannot be directly assessed because of the high degree of cancellation between the eddy forcing and the mean meridional circulation induced by the eddies. The general subject of wave-mean flow interaction has recently been elucidated in a fundamental way by Andrews and McIntyre (1978) who employ a hybrid Eulerian-Lagrangian theory [see McIntyre (1980) for a good introduction to the theory]. Their theory requires that wave disturbances be described in terms of fluid particle displacements about the mean flow, rather than in terms of the usual Eulerian perturbation velocity fields. This approach partitions the motions between eddy and mean flow components in a manner which is more appropriate for evaluating the net forcing of the mean flow by the eddies. Unfortunately, however, there are a number of technical difficulties associated with applying the Lagrangian averaging scheme as a diagnostic tool in the present model where wave-related displacements become very large.[4]

An alternative diagnostic scheme, which overcomes some of the problems of the traditional Eulerian averaging, but does not require evaluation of the parcel displacements, was introduced by Andrews and McIntyre (1976). They defined a "residual" mean meridional circulation which in terms of our density weighted variables is given by the streamfunction

$$\bar{\chi}_R \equiv \bar{\chi} + B/N^2, \tag{21}$$

where

$$B \equiv e^{z/2H}\cos\theta\left[V_S\left(\frac{\partial}{\partial z}+\frac{1}{2H}\right)\Psi_S^* + V_S^*\left(\frac{\partial}{\partial z}+\frac{1}{2H}\right)\Psi_S\right]$$

is the horizontal eddy heat flux. The residual mean vertical velocity is given by

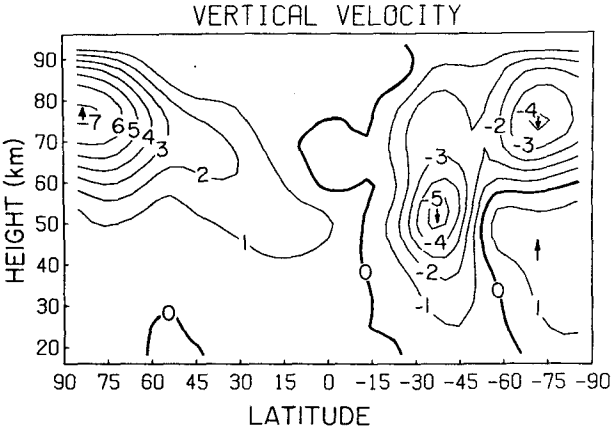

FIG. 18. Mean vertical velocity (mm s^{-1}) at Northern Hemisphere summer solstice.

$$\bar{W}_R = \bar{W} + \frac{1}{N^2\cos\theta}\frac{\partial B}{\partial y} \tag{22}$$

and the residual mean meridional velocity is

$$\bar{V}_R = \bar{V} - \frac{1}{\cos\theta}\left(\frac{\partial}{\partial z}-\frac{1}{2H}\right)\left(\frac{B}{N^2}\right). \tag{23}$$

Thus, the residual mean circulation is just that part of the mean meridional circulation which is not exactly balanced by the horizontal eddy heat flux divergence.

Substituting from (22) and (23) into (5) and (2), we obtain

$$\frac{\partial}{\partial t}\left(\frac{\partial\bar{\Psi}}{\partial z}+\frac{\bar{\Psi}}{2H}\right) + N^2\bar{W}_R = \bar{Q} + \{\text{other terms}\}, \tag{24}$$

$$\frac{\partial\bar{U}}{\partial t} - f\bar{V}_R = \bar{P} - \kappa_R\bar{U} + \{\text{other terms}\}, \tag{25}$$

where

$$\bar{P} \equiv F_M + \frac{f}{\cos\theta}\left(\frac{\partial}{\partial z}-\frac{1}{2H}\right)B/N^2$$

is (for planetary waves) approximately equal to the quasi-geostrophic potential vorticity flux (Holton, 1975).[5]

In general, the "other terms" (nonlinear advection and dissipation) in (24) and (25) are of secondary importance. Therefore, to a first approximation, for steady conditions, the residual mean vertical velocity just balances the diabatic heating $\bar{Q}$ and may be identified as the "diabatic circulation." Dunkerton (1978) has shown that this circulation is more relevant to the transport of tracers in the stratosphere

[4] McIntyre (1980) discusses this problem in detail.

[5] $\bar{P}$ is also approximately equal to the divergence of the so-called Eliassen-Palm flux (Andrews and McIntyre, 1976).

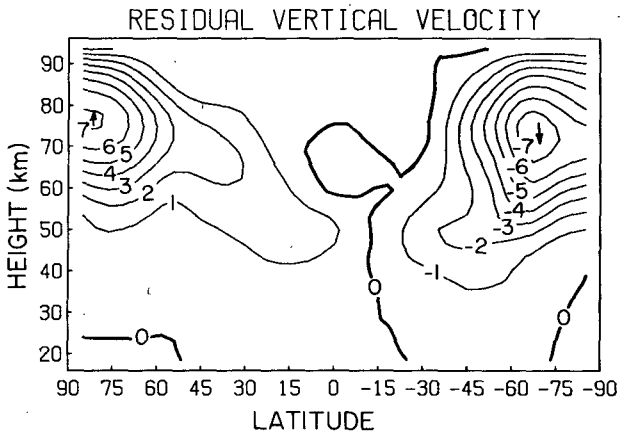

FIG. 19. Residual mean vertical velocity (mm s^{-1}) at Northern Hemisphere summer solstice.

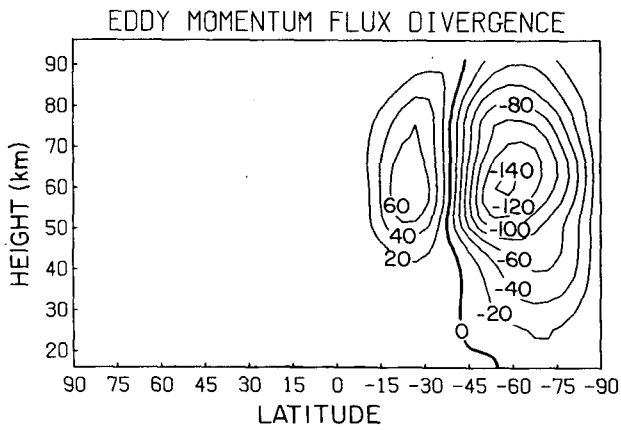

FIG. 21. Eddy momentum flux divergence (10^{-6} m s^{-2}) at Northern Hemisphere summer solstice.

and mesosphere than is the Eulerian mean meridional motion.

In the present model the motion is approximately steady at the Southern Hemisphere winter solstice. Figs. 19 and 20 show the residual mean meridional circulation for that time. A comparison with Figs. 12 and 14 of HW indicates that the residual mean velocities ($\bar{V}_R, \bar{W}_R$) are nearly identical to the mean meridional velocities computed for the same season in the two-dimensional model. This supports the arguments given in HW that the mean meridional circulation of the two-dimensional model should be interpreted as the *diabatic* circulation, since for steady conditions the adiabatic cooling $N^2\bar{W}_R$ must nearly balance the diabatic heating $\bar{Q}$. As this approximate balance holds in both the HW model and the present model, we may conclude that the eddy forcing has very little effect on the solstice mean temperature field.

Because the mean zonal wind and zonal mean temperature fields are in approximate thermal wind balance the above argument would seem to imply that the eddy forcing should also have little influence on the mean zonal wind distribution at the solstices. Indeed, this is the case at high latitudes as can be seen by comparing Fig. 8 with Fig. 7 of HW. However, at low latitudes, where only small temperature gradients are required to maintain thermal wind balance, large differences occur.[6] The subtropical winter mean zonal winds are much weaker in the present case.

In the HW model the solstice season momentum budget was satisfied by a near balance between the Coriolis torque of the mean meridional wind and the Rayleigh frictional dissipation. Thus in the stratosphere and lower mesosphere, where the Rayleigh friction coefficient was small, relatively large mean zonal winds were required to establish the balance

$$f\bar{V} \approx \kappa_R \bar{U}.$$

In the present model a third term, the eddy potential vorticity flux $\bar{P}$, must be included in the momentum budget as shown in (25).

The potential vorticity flux is given by the sum of the eddy momentum flux divergence plus the vertical gradient of the eddy heat flux. For steady waves in the absence of dissipation, quasi-geostrophic theory predicts that these two terms should exactly balance so that the net potential vorticity flux vanishes (Dickinson, 1969). The tendency for cancellation is clearly present in our model (below 70 km) as can be seen by comparing Figs. 21 and 22 which show the eddy momentum flux divergence and the potential vorticity flux, respectively. In high latitudes the potential vorticity flux, and hence the net mean flow forcing, is very small so that the mean

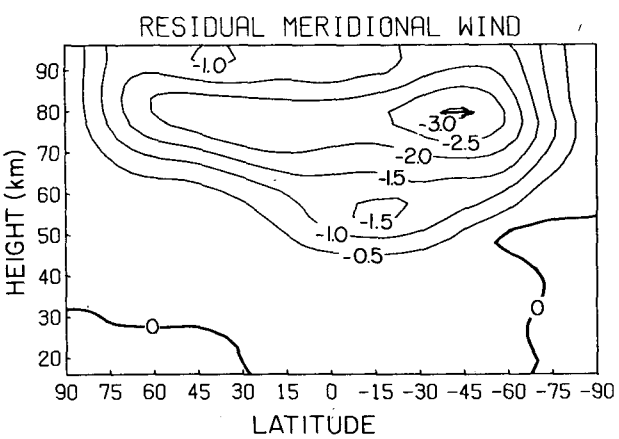

FIG. 20. Residual mean meridional wind (m s^{-1}) at Northern Hemisphere summer solstice.

[6] As mentioned in Section 4a the large vertical scale of the zonal wind deceleration is an additional factor contributing to the small influence of the waves on the thermal field.

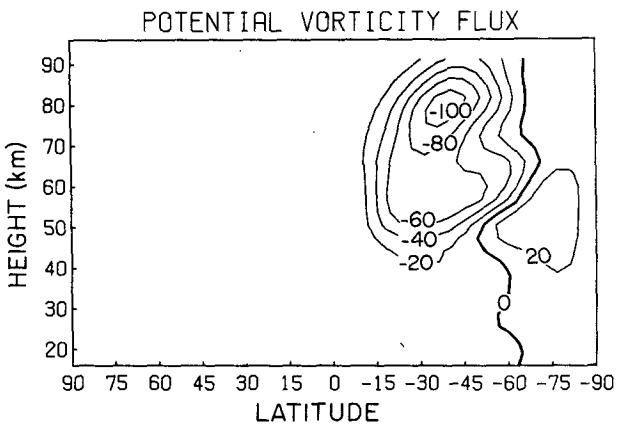

FIG. 22. Quasi-geostrophic potential vorticity flux (10^{-6} m s^{-2}) at Northern Hemisphere summer solstice.

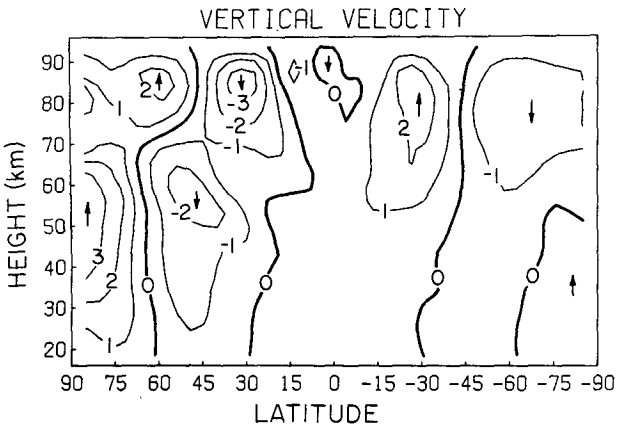

FIG. 23. Mean vertical velocity (mm s^{-1}) at Northern Hemisphere vernal equinox.

zonal flow and the residual mean meridional wind are both similar to the corresponding high-latitude fields in the HW model. In low and middle latitudes, however, there is a substantial negative potential vorticity flux. This negative potential vorticity flux partly balances the Coriolis torque due to the residual mean meridional wind. Thus, for a given $\bar{V}_R$ a smaller $\bar{U}$ is required to maintain the zonal mean momentum budget than would be the case if no eddy forcing were present. It is for this reason that the mean zonal winds can remain quite weak in the low latitudes of the winter hemisphere in the present model.

Equatorward of 30° the potential vorticity flux is nearly equal to the eddy momentum flux convergence, indicating that *horizontal* wave propagation toward the equator is an essential process controlling the mean flow distribution in that region. The meridional wave propagation toward the equator, combined with the inability of the waves to propagate past the $\bar{U} = 0$ critical line, leads to the strong eddy momentum flux divergence in this region. It is also notable that the $\bar{U} = 0$ line is located at nearly the same latitude at the solstices in the present model as it was in HW, suggesting that [in agreement with the results of Beland, (1976)] the wave eddy fluxes are not able to cause a significant lateral propagation of the critical line.[7]

In midlatitudes above 70 km there is a strong negative flux of potential vorticity where the eddy momentum flux divergence is small. The potential vorticity flux in this region is due to the vertical gradient of the poleward eddy heat flux as the waves encounter strong mechanical dissipation near the mesopause. Again, the negative potential vorticity flux partly balances the Coriolis torque $\bar{V}_R$ so that the equilibrium mean zonal wind is weaker in this region than in the HW model.

6. The Northern Hemisphere final warming

Although only minor midwinter warmings occurred during the simulation, a major sudden warming occurred near the spring equinox in the Northern Hemisphere. In the period from 40 to 10 days prior to the equinox the polar temperature at 48.5 km rose 18°C (see Fig. 2) compared to a rise of 3°C for the same period in the HW model. This warming was associated with an increase in the amplitude of the wavenumber 1 geopotential perturbation between 40 and 60 km (Fig. 11) followed by a rapid decay when the mean winds became easterly in the polar region. Both wave damping

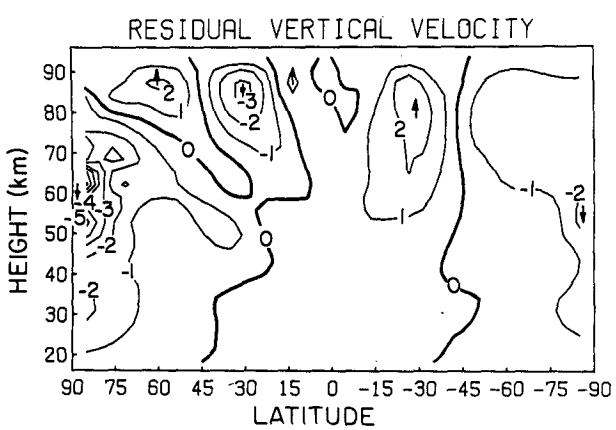

FIG. 24. Residual mean vertical velocity (mm s^{-1}) at Northern Hemisphere vernal equinox.

[7] It should be noted that our 10° latitude grid spacing is much too crude to resolve the detailed structure of the critical layer region, and that the critical layer must therefore be partially reflecting in our model despite the absence of nonlinearity. However, according to Tung (1979) planetary wave critical layers in the atmosphere probably *are* partially reflecting, so that the lack of resolution in the critical layer may not be serious.

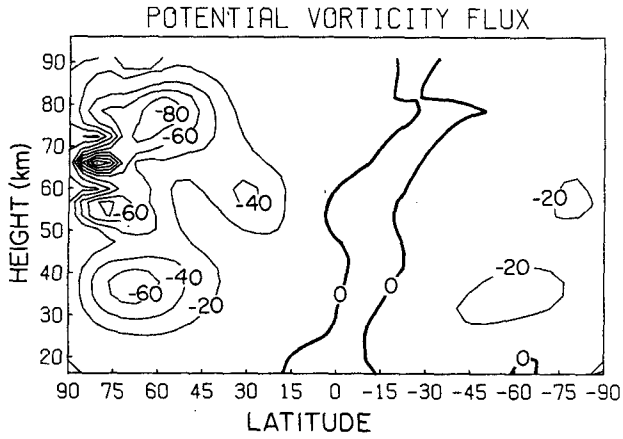

FIG. 25. Potential vorticity flux (10^{-6} m s^{-2}) at Northern Hemisphere vernal equinox.

and wave transience appear to be responsible for this final warming. The easterly acceleration in the upper mesosphere associated with the warming process is rather weak because strong mechanical dissipation of the mean flow tends to balance the negative potential vorticity flux for an easterly mean wind [see Eq. (25)].

The vertical velocity and residual vertical velocities for the equinox are given in Figs. 23 and 24, respectively. The corresponding potential vorticity flux is shown in Fig. 25. The vertical velocity pattern is more complicated than the solstice pattern shown in Fig. 18 partly due to the presence of transient zonally symmetric inertia-gravity wave oscillations above 70 km. In the stratosphere there are thermally indirect cells at high latitudes in both hemispheres. However, by far the much stronger cell exists in the Northern hemisphere where there is an intense equatorward potential vorticity flux. The residual vertical velocity pattern in the stratosphere, however, consists of a single thermally direct cell in each hemisphere with rising motion in the tropics and sinking at high latitudes. Although this pattern is in qualitative agreement with HW, the subsidence in the Northern Hemisphere is greater by a factor of 3 than in the HW mode. This strong subsidence would create a more rapid warming if it were not partly balanced by the strong diabatic cooling which the anomalously warm polar region undergoes at this time.

7. Concluding remarks

We have shown that a global primitive equation model which is severely truncated zonally to retain only the zonal mean and a single zonal harmonic wave component can be used to simulate many features of the annual cycle of the zonal mean circulation in the middle atmosphere. In particular, we find that the forced planetary wavenumber 1 disturbances play a far more important role in the momentum budget than in the thermal budget. Thus, in addition to vertical propagation, horizontal (meridional) wave propagation is crucially important for understanding the dynamics of the middle atmosphere.

In order to diagnose the model and to compare the results with the HW two-dimensional model, we have used the residual mean meridional circulation defined by Andrews and McIntyre (1976) in combination with the potential vorticity flux. We find that these derived fields provide much clearer insights into the dynamics of wave-mean flow interaction than the conventional Eulerian fields.

The present model, with its time-independent forcing of planetary wavenumber 1, has revealed some interesting asymmetries between the hemispheres apparently due to the great sensitivity of the waves to the mean zonal wind profile, and especially to the mean zonal wind at the lower boundary. However, in the present model no aperiodic vacillations (e.g., mid-winter major warmings) occurred. Previous experiments such as those of Schoeberl and Strobel (1980) suggest that planetary wavenumber 2 forcing should be much more effective in producing transient variations such as sudden warmings. A companion experiment involving wavenumber 2 forcing will be reported later.

Acknowledgments. We wish to thank Professor Conway Leovy, Dr. Michael E. McIntyre and Professor Taroh Matsuno for helpful suggestions. Dr. John Barnett kindly supplied the original print for Fig. 3a. This work was supported by the National Aeronautics and Space Administration under NASA Grant NSG-2228.

REFERENCES

Andrews, D. G., and M. E. McIntyre, 1976: Planetary waves in horizontal and vertical shear: The generalized Eliassen-Palm relation and the zonal mean acceleration. *J. Atmos. Sci.*, **33**, 2031–2048.

——, and ——, 1978: An exact theory of nonlinear waves on a Lagrangian-mean flow. *J. Fluid Mech.*, **89**, 609–646.

Barnett, J. J., 1974: The mean meridional behavior of the stratosphere from November 1970 to November 1971 derived from measurements by the Selective Chopper Radiometer on Nimbus 4. *Quart. J. Roy. Meteor. Soc.*, **100**, 505–530.

Beland, M., 1976: Numerical study of the nonlinear Rossby wave critical level development in a barotropic zonal flow. *J. Atmos. Sci.*, **33**, 2065–2078.

Boyd, J., 1976: The noninteraction of waves with the zonally averaged flow on a spherical earth and the interrelationships of eddy fluxes of energy, heat, and momentum. *J. Atmos. Sci.*, **33**, 2285–2291.

Charney, J. G., and P. G. Drazin, 1961: Propagation of planetary scale wave disturbances from the lower into the upper atmosphere. *J. Geophys. Res.*, **66**, 83–109.

Cogley, A. C., and W. J. Borucki, 1976: Exponential approximation for daily average solar heating or photolysis. *J. Atmos. Sci.*, **33**, 1347–1356.

Cunnold, D. M., F. Alyea, N. Phillips and R. Prinn, 1975: A

three-dimensional dynamical chemical model of atmospheric ozone. *J. Atmos. Sci.*, **32**, 170–194.

Dickinson, R. E., 1969: Theory of planetary wave-zonal flow interaction. *J. Atmos. Sci.*, **26**, 73–81.

——, 1973: Method of parameterization for infrared cooling between altitudes of 30 and 70 km. *J. Geophys. Res.*, **78**, 4451–4457.

Dunkerton, T., 1978: On the mean meridional motions of the stratosphere and mesosphere. *J. Atmos. Sci.*, **35**, 2325–2333.

Hirota, I., and J. J. Barnett, 1977: Planetary waves in the winter mesosphere—preliminary analysis of the Nimbus 6 PMR results. *Quart. J. Roy. Meteor. Soc.*, **103**, 487–498.

Holton, J. R., 1975: *The Dynamic Meteorology of the Stratosphere and Mesosphere. Meteor. Monogr.*, No. 37, Amer. Meteor. Soc., 218 pp.

——, 1979: *An Introduction to Dynamic Meteorology*, 2nd ed. Academic Press, 391 pp.

——, and T. Dunkerton, 1978: On the role of wave transience and dissipation in stratospheric mean flow vacillations. *J. Atmos. Sci.*, **35**, 740–744.

——, and W. M. Wehrbein, 1980: A numerical model of the zonal mean circulation of the middle atmosphere. *Pure Appl. Geophys.*, **118**, 284–306.

Houghton, J. T., 1978: The stratosphere and mesosphere. *Quart. J. Roy. Meteor. Soc.*, **104**, 1–29.

Lacis, A. A., and J. E. Hansen, 1974: A parameterization for the absorption of solar radiation in the earth's atmosphere. *J. Atmos. Sci.*, **31**, 118–133.

Leovy, C. B., 1964: Simple models of thermally driven mesospheric circulation. *J. Atmos. Sci.*, **21**, 327–341.

Mahlman, J. D., 1969: Heat balance and mean meridional circulation in polar stratosphere during warming of January 1958. *Mon. Wea. Rev.*, **97**, 534–540.

Matsuno, T., 1971: A dynamical model of the stratospheric sudden warming. *J. Atmos. Sci.*, **28**, 1479–1494.

McIntyre, M. E., 1979: An introduction to the generalized Lagrangian-mean description of wave-mean flow interaction. *Pure Appl. Geophys.*, **118**, 152–176.

——, 1980: Towards a Lagrangian-mean description of stratospheric circulations and chemical transports. *Phil. Trans. Roy. Soc. London*, **A296**, 129–148.

Schoeberl, M. R., and D. F. Strobel, 1978: The zonally averaged circulation of the middle atmosphere. *J. Atmos. Sci.*, **35**, 577–591.

——, and ——, 1980: Numerical simulation of sudden stratospheric warmings. *J. Atmos. Sci.*, **37**, 214–236.

Simmons, A. J., B. J. Hoskins and D. M. Burridge, 1978: Stability of the semi-implicit method of time integration. *Mon. Wea. Rev.*, **106**, 405–412.

Trenberth, K. E., 1973: Global model of the general circulation of the atmosphere below 75 km with an annual heating cycle. *Mon. Wea. Rev.*, **101**, 306–322.

Tung, K. K., 1979: A theory of stationary long waves. Part III: Quasi-normal modes in a singular wave guide. *Mon. Wea. Rev.*, **107**, 751–774.

Wallace, J. M., 1978: Trajectory slopes, countergradient heat fluxes, and mixing by lower stratospheric waves. *J. Atmos. Sci.*, **35**, 554–558.